# Estimation of Chlorophyll a Concentration Using NIR/Red Bands of MERIS and Classification Procedure in Inland Turbid Water

Yunmei Li, Qiao Wang, Chuanqing Wu, Shaohua Zhao, Xing Xu, Yanfei Wang, and Changchun Huang

***Abstract*—The classification criteria are established to classify the water of Taihu Lake into four classes based on above-water remote sensing reflectance ($R_{\mathrm{rs}}$), i.e., types A to D. Among the four water types, type A spectra represented the case of waters where algal blooms or aquatic plants appeared, while type B is referred to the water with high suspended matter concentration and low chlorophyll a concentration ($C_{\mathrm{chla}}$). Both types A and B were not suitable for retrieving $C_{\mathrm{chla}}$ from image data. Hence, three-band, four-band, and two-band ratio algorithms were constructed to retrieve $C_{\mathrm{chla}}$ from water types C and D. The obtained results showed that the relation trends between $C_{\mathrm{chla}}$ and $R_{\mathrm{rs}}$ were different between type C and type D waters. By using Medium Resolution Imaging Spectrometer images, acquired on November 11, 2007 and November 20, 2008, the $C_{\mathrm{chla}}$ of Taihu Lake was mapped by band 9/band 7 models; it could be concluded that the $C_{\mathrm{chla}}$ mainly ranged from 0 to 20 mg $\cdot$ m$^{-3}$, accounting for 83.70% of the whole lake area in 2007 image, while the area was 86.63% in 2008 image. The estimation accuracies varied from different $C_{\mathrm{chla}}$ ranges. The *mean absolute percent errors* obtained by band 9/band 7 models were 106.23%, 56.79%, 38.04%, 33.80%, and 58.74% for the ranges 0 mg $\cdot$ m$^{-3}$ $< C_{\mathrm{chla}} <=$ 5 mg $\cdot$ m$^{-3}$, 5 mg $\cdot$ m$^{-3}$ $< C_{\mathrm{chla}} <=$ 10 mg $\cdot$ m$^{-3}$, 10 mg $\cdot$ m$^{-3}$ $< C_{\mathrm{chla}} <=$ 20 mg $\cdot$ m$^{-3}$, 20 mg $\cdot$ m$^{-3}$ $< C_{\mathrm{chla}} <=$ 30 mg $\cdot$ m$^{-3}$, and 30 mg $\cdot$ m$^{-3}$ $< C_{\mathrm{chla}}$, respectively. Correspondingly, the *root-mean-square errors* were 5.02, 4.45, 5.59, 8.72, and 32.55 mg $\cdot$ m$^{-3}$, respectively.**

***Index Terms*—Chlorophyll a concentration, Medium Resolution Imaging Spectrometer (MERIS), near infrared (NIR)/red model, Taihu Lake, water classification.**

## I. Introduction

As THE THIRD largest freshwater lake in China, Taihu Lake is very important for water supply to major cities along the lakeshore. However, water pollution of the lake is becoming more and more serious in recent years, which has caused lake eutrophication. This problem severely threatens the normal functioning of the lake. As such, it is essential that the water quality should be regularly monitored for tracking the anthropogenic effects and sustainably managing water resource. Fortunately, as a key indicator of water quality, chlorophyll a concentration ($C_{\mathrm{chla}}$) can be inversed from remotely sensed data, which is crucial for the continuous monitoring of water quality. Generally speaking, the $C_{\mathrm{chla}}$ can be derived from the blue and green spectral bands [1], [2] in open-ocean Case-1 water. However, the method is not very suitable for inland productive turbid waters, because of the overlapping and uncorrelated absorptions by dissolved organic matter and nonalgal particles in the blue spectral region [3]–[6]. Thus, spectral algorithms which are based on reflectance in the red and the near-infrared (NIR) spectral regions are regarded to be preferable for estimating $C_{\mathrm{chla}}$ in turbid productive waters [6]–[9]. Dall'Olmo *et al.* [6] validated the potential of applying NIR/red reflectance ratios to estimate $C_{\mathrm{chla}}$ via Sea-viewing Wide Field-of-view Sensor and Moderate Resolution Imaging Spectroradiometer data. Gons [8] developed a simple semianalytical method using wavebands centered at 665, 705, and 775 nm and later reexamined the performance by setting wavelength 708.75 nm instead of 705 nm [10]. Dall'Olmo and Gitelson [11] developed a three-band semianalytical algorithm for estimating $C_{\mathrm{chla}}$. Moses *et al.* [12] validated a three-band model and a two-band model which used Medium Resolution Imaging Spectrometer (MERIS) reflectances in the red and NIR spectral regions for estimating $C_{\mathrm{chla}}$ in inland, estuarine, and coastal turbid productive waters. Some studies show that three-band model is better than the two-band ratio [13], [14].

Three-band algorithm is based on radiative transfer (RT) theory according to absorption and scattering properties of water constituents. The relationship between $C_{\mathrm{chla}}$ and three band is as follows:

$$C_{\mathrm{chla}} \propto \left[R_{\mathrm{rs}}^{-1}(\lambda_1) - R_{\mathrm{rs}}^{-1}(\lambda_2)\right] \times R_{\mathrm{rs}}(\lambda_3) \qquad (1)$$

where $R_{\mathrm{rs}}(\lambda_i)$ stands for remote sensing water reflectance at wavelength $\lambda_i$ ($i = 1, 2$ or 3), usually in the visible range of 400–800 nm.

The efficiency of the algorithm has been proved in various lakes and reservoirs with variable optical properties [12]–[15], and the algorithm is also validated in Taihu Lake [16], [17].

Manuscript received November 1, 2010; revised February 26, 2011 and May 1, 2011; accepted July 17, 2011. Date of publication September 15, 2011; date of current version February 24, 2012. This work was supported in part by the National Natural Science Foundation of China under Grant 40971215, by National Doctoral Fund under Grant 20093207110011, and by the Special Project of High-Resolution under Grant E0203/1112.

Y. Li, X. Xu, Y. Wang, and C. Huang are with the Key Laboratory of Virtual Geographic Environment, Ministry of Education, Nanjing Normal University, Nanjing 210046, China (e-mail: liyunmei@njnu.edu.cn; 68698500@qq.com; 357008144@qq.com; huangchangchun_aaa@163.com).

Q. Wang, C. Wu, and S. Zhao are with the Satellite Environment Application Center, Ministry of Environmental Protection, Beijing 100029, China (e-mail: wangqiao@sepa.gov.cn; wu.chuanqing@sepa.gov.cn; zshyytt@126.com).

Color versions of one or more of the figures in this paper are available online at http://ieeexplore.ieee.org.

Digital Object Identifier 10.1109/TGRS.2011.2163199

The MERIS data consisting of 15 spectral channels [19] enable accurate monitoring of the Earth's atmosphere and surface [20]. Among these channels, bands 7–11 (i.e., band 7: 660–670 nm; band 8: 677.5–685 nm; band 9: 703.75–713.75 nm; band 10: 750–757.5 nm; and band 11: 758.75–762.5 nm) are within the optimal ranges for pigment retrievals suggested by Gitelson *et al.* [14]. This makes it possible to apply the three-band algorithm to MERIS image data. However, the efficiency of the lower spectral resolution compared with field spectrophotometer still remains to be validated [12].

In addition, the remote sensing reflectances ($R_{\rm rs}$'s) vary widely in the spectral shape and magnitude, even in the same water body, such as Taihu Lake [21]–[23]. For example, some subregions of the lake are mainly influenced by phytoplankton, while the others by inorganic suspended particle or even by floating algae [24], [25]. As a result, the sensitivity of $R_{\rm rs}$ to $C_{\rm chla}$ changes with different water bodies. Therefore, it is very necessary to establish specific $C_{\rm chla}$ retrieval algorithms for specific water optical characteristics.

In this paper, we classified the $R_{\rm rs}$ of Taihu Lake into four classes relying on MERIS bands and then established NIR/red algorithms for different water classes. The objective of this paper is to test the NIR/red algorithms (i.e., three-band models, four-band models, and band ratio models at NIR/red wavebands) based on MERIS imagery for Taihu Lake. The specific goals are the following: 1) to classify water types based on $R_{\rm rs}$ characteristics; 2) to establish NIR/red algorithms for estimating $C_{\rm chla}$ based on water types; and 3) to inverse $C_{\rm chla}$ from MERIS image data.

## II. Material and Methods

### A. Study Area and Sampling

The study area is Taihu Lake, one of the largest freshwater lakes in China. Taihu Lake, located between $30°56' - 31°33'$ N and $119°53' - 120°36'$ E, has a water area of 2338 km$^2$ and an average depth of about 1.9 m [26]. In recent years, algal blooms have been occurring nearly during the whole year, and the density of cyanobacteria has been particularly high from May to October [27].

Surface water samples were collected using Niskin bottles at stations distributed evenly over the entire lake during October 24, 2006–November 4, 2006, November 8–21, 2007, November 10–21, 2008, and April 17–28, 2009 (Fig. 1) (The numbers of useful samples, considering the weather conditions, were 53, 46, 61, and 54 in 2006, 2007, 2008, and 2009, respectively). They were immediately deep frozen and brought back to laboratory for analysis within the same day.

### B. In Situ Measurements of Hyperspectral Reflectance

Reflectance spectra were measured above water using a portable ASD FieldSpec spectroradiometer between 10:00 and 14:00 h local time. With a viewing field of 25°, this instrument has a sensitivity ranging from 350 to 1050 nm at an increment of 1.58 nm with 512 wavebands. The measurement of water surface reflectance spectra followed the method described by

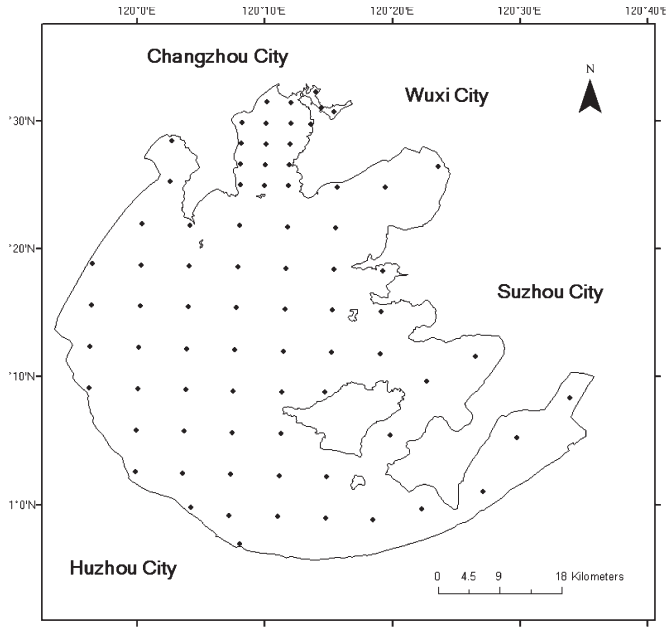


Fig. 1. Distribution of sample stations in the study area. N is latitude north; E is longitude east. The numbers of measured stations in 2006, 2007, 2008, and 2009 were 53, 46, 61, and 54, respectively.

Mueller *et al.* [28] and Le *et al.* [16]. When the boat was anchored, the radiance spectra of the reference panel ($L_p$), water ($L_{\rm sw}$), and the sky ($L_{\rm sky}$) were measured ten times each, and the spectra at each sampling station were averaged to derive remote sensing reflectance $R_{\rm rs}(\lambda)$. In order to effectively avoid the interference of the ship with the water surface and the influence of direct solar radiation, the instrument was positioned at an angle of 90°–135° with the plane of the incident radiation away from the sun. The view of the water surface was controlled between 30° and 45° with the aplomb direction. In this way, most of the direct sunlight was eliminated while the impact of the ship's shadow was minimized. Immediately after measuring the water radiance, the spectroradiometer was rotated upward by 90°–120° to measure the skylight radiance ($L_{\rm sky}$). The view azimuth angle in this measurement was kept the same as that in measuring water radiance. $R_{\rm rs}(\lambda)$ was calculated as

$$R_{\rm rs} = L_w / E_d(0^+) \tag{2}$$

where $L_w$ is the water-leaving radiance and $E_d(0^+)$ is the total incident radiant flux of the water surface.

$L_w$ and $E_d(0^+)$ in (2) were further computed as

$$L_w = L_{\rm sw} - rL_{\rm sky} \tag{3}$$

where $L_{\rm sw}$ stands for the total radiance received from the water surface; $L_{\rm sky}$ refers to diffuse radiation of the sky, which contains no information on water properties and, hence, has to be eliminated; and $r$ represents the reflectance of the skylight at the air–water interface [29]. Its value depends upon solar azimuth, measurement geometry, wind speed, and surface roughness. Here, $r = 2.26\%$

$$E_d(0^+) = \pi L_p / \rho_p \tag{4}$$

where $L_p$ is the radiance of the gray board and $\rho_p$ stands for the reflectance of the gray board, which is very close to 30% and was provided by the manufacturer.

To match with MERIS data, the $R_{\rm rs}$ data were resampled to MERIS bands 1–12 (i.e., band 1: 407.5–417.5 nm; band 2: 437.5–447.5 nm; band 3: 485–495 nm; band 4: 505–515 nm; band 5: 555–565 nm; band 6: 615–625 nm; band 7: 660–670 nm; band 8: 677.5–685 nm; band 9: 703.75–713.75 nm; band 10: 750–757.5 nm; band 11: 758.75–762.5 nm; and band 12: 771.25–786.25 nm.).

### C. Measurements of Concentration

The $C_{\rm chla}$ and the total suspended matter concentrations $(C_{\rm tsm})$ were measured according to the lake investigation criteria in China [30]. Chlorophyll a was extracted with ethanol (90%) at 80 °C and analyzed spectrophotometrically at 750 and 665 nm, with correction for phaeopigments [31].

### D. MERIS Data and Atmospheric Correction

Full-resolution (FR) images with 300-m spatial resolution, acquired on November 11, 2007 and November 20, 2008, were used in this study.

One challenge for reliable retrieval of optical parameters over Case-2 waters is the accurate atmospheric correction [32]. Automated procedures to derive aerosol concentration from ocean color sensors over Case-1 waters using the dark pixel correction [33], which assume zero water-leaving radiance in the near infrared, are not suitable for Case-2 waters [34] and easily lead to the presence of negative water-leaving radiance in the blue. Therefore, for remote sensing of Case-2 waters, new approaches for the atmospheric correction are required because there is no wavelength in the reflectance spectra at which the water-leaving radiance is zero. Three plug-in algorithms were developed for BEAM—the basic ENVISAT toolbox for MERIS (both BEAM and plug-in can be downloaded freely from the BEAM Project home page http://www.Brockmann-consult.de/beam/) based on the MERIS Case-2 Core Module, i.e., Case-2 Regional [35], boreal lakes, eutrophic lakes and a dedicated atmospheric correction [36]. These algorithms, based on the trained artificial neural network (ANN), can retrieve the remote sensing reflectance $(R_{\rm rs})$ at the bottom-of-atmosphere (BOA) from MERIS Level 1b top-of-atmosphere (TOA) radiances and then generate the inherent optical properties and subsequently the concentrations of water constituents by the BOA $R_{\rm rs}$. The construction of the plug-in algorithms for BOA $R_{\rm rs}$ derivation includes two steps as follows. The first step involves the building up of the training data set, and the second step involves the construction of ANN inverse model [35], [36].

However, when the algorithms were applied to Taihu Lake, they were not so good because those algorithms were specifically derived from European coastal water or inland lake. That means that their simulated databases are not suitable to the highly turbid and eutrophic Taihu Lake. To enhance the accuracy of atmospheric correction, the input parameters were set according to the premier study of Taihu Lake [37], and the local training data set was built via the simulation of TOA radiances by 6S model. Hu [37] studied the aerosol property in Taihu Lake area and proposed that the proportion of the aerosol constituents in summer and winter was as follows: 1) dustlike as 0.5, water soluble as 0.29, oceanic as 0.00, and soot as 0.21 in summer; 2) dustlike as 0.48, water soluble as 0.5, oceanic as 0.00, and soot as 0.02 in winter. Therefore, in our study, the input parameters for the forward simulating 6S model were as follows:

1) geometrical conditions: mean values of altitude and solar and sensor zenithal and azimuthal angles of the images;
2) atmospherical models: atmospheric conditions obtained from image metadata, such as mean pressure, mean temperature, mean water density, and mean ozone density. In addition, the volume percentages of aerosol components were the following: dustlike ranged from 0.4 to 0.5, water soluble ranged from 0.2 to 0.5, oceanic was zero, soot ranged from 0.00 to 0.2, and the step was 0.1 for each constituent;
3) ground reflectance: *in situ* measured $R_{\rm rs}$ in 2007 and 2008.

Therefore, the forward model included several atmospheric property parameters as inputs to make the training data set. Then, a feedforward back-propagation ANN model was trained by the data set using a neural network tool of Matlab's toolbox for MERIS bands 1–10 and band 12. Thereafter, the smile-corrected MERIS image data were input into the trained ANN to retrieve BOA $R_{\rm rs}$.

### E. Chlorophyll a Concentration Retrieval Models

The optimal NIR/red bands and corelationships of inland waters vary with different data sets based on their optical properties [14]–[18]. Thus, it is hard to build a uniform algorithm for various inland waters. However, if the waters had similar optical properties, the same algorithm might be applied to different waters or seasons. Based on that assumption, we first classified the waters into different types relying on $R_{\rm rs}$ and then established NIR/red models according to the relationships between $R_{\rm rs}$ and NIR/red bands.

It is preferable to use concurrent *in situ* and image data to establish $C_{\rm chla}$ retrieval model. However, in fact, the temporal and spatial differences between the *in situ* and satellite data make it difficult to calibrate the models [12]. Therefore, in this study, the three-band, four-band and two-band ratio models were constructed using *in situ* measured data sets in 2007 and 2008, while the data sets measured in 2006 and 2009 and the image data acquired in 2007 and 2008 were used for validation.

The mean absolute percent error *(MAPE)* and root-mean-square error *(RMSE)* between measured and predicted values were calculated for model accuracy evaluation

$$MAPE = \frac{1}{n}\sum_{i=1}^{n}\left|\frac{y_i - y_i'}{y_i}\right| \tag{5}$$

$$RMSE = \sqrt{\frac{1}{n}\sum_{i=1}^{n}(y_i - y_i')^2} \tag{6}$$

TABLE I
*MAPEs* BETWEEN MEASURED AND RETRIEVED BOA $R_{rs}$ IN 2007 AND 2008 DATA SETS

| Band | | 1 | 2 | 3 | 4 | 5 | 6 | 7 | 8 | 9 | 10 | 12 |
|---|---|---|---|---|---|---|---|---|---|---|---|---|
| *MAPE* (%) | 2007 | 28.92 | 24.35 | 23.38 | 22.72 | 18.35 | 16.80 | 17.40 | 19.91 | 37.88 | 42.83 | 42.85 |
| | 2008 | 23.45 | 21.21 | 18.57 | 16.92 | 21.64 | 23.14 | 21.89 | 17.80 | 32.31 | 50.93 | 58.53 |

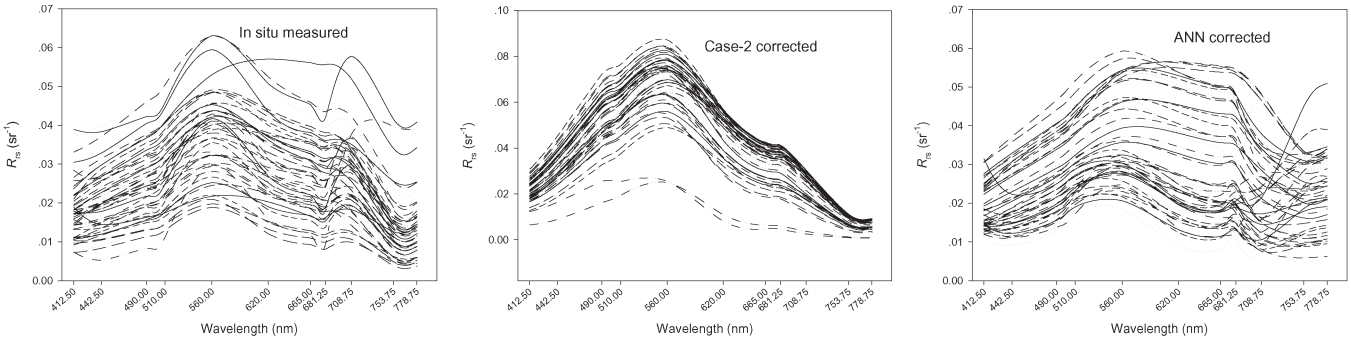


Fig. 2. *In situ* measured, Case-2 plug-in corrected, and ANN corrected $R_{rs}$.

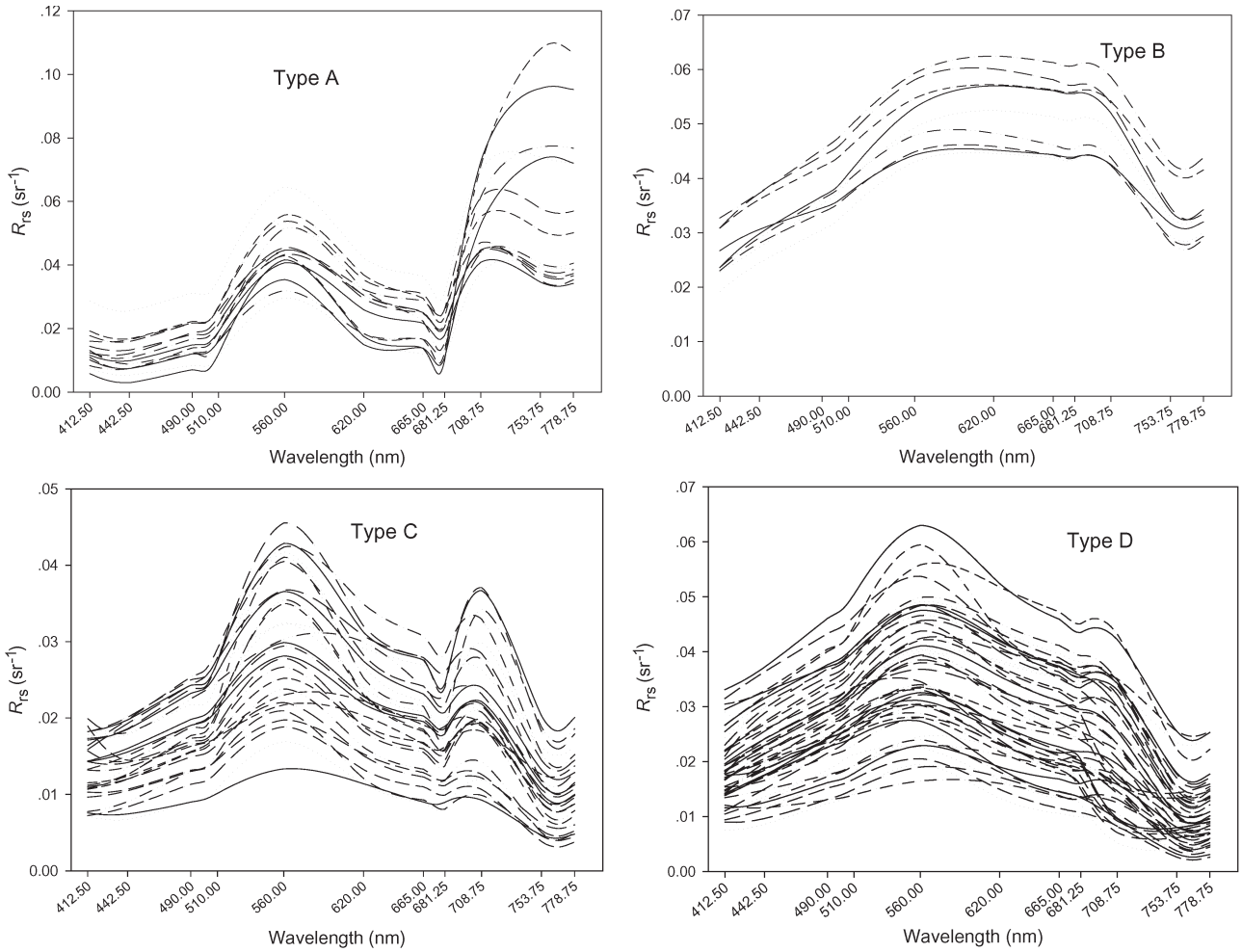


Fig. 3. Water types in Taihu Lake.

where $n$ is the number of samples, $y_i$ is the measured value, and $y_i'$ is the estimated value.

## III. Results

### A. Atmospheric Correction Validation

A four-layer feedforward backpropagation ANN model with 11 input and output neurons was trained by the simulated TOA radiance reflectance and *in situ* measured $R_{\rm rs}$. Then, two image data of 2007 and 2008 were smile corrected by using BEAM version 4.7, and then, they were input into the trained ANN to retrieve BOA $R_{\rm rs}$. To avoid the regions with strongly spatial variation of water optical properties or potentially high residual noise from the atmospheric correction, only those samples at which the variance of nine neighbor pixels less than 10% was used to evaluate the atmospheric correction accuracy. The *MAPEs* between the measured and retrieved data are shown in Table I. Moreover, the *MAPE* data indicated that, from visible to NIR bands, the accuracy declined due to relatively low water reflectance and therefore comparatively high noise [38]. Nevertheless, when compared with the BEAM's plug-in algorithm, the locally trained ANN produced a significantly better result in preserving the distinct shapes of the reflectance features between bands 7 and 12 in the $R_{\rm rs}$ spectra (Fig. 2).

### B. Water Classification

Based on the observation of the spectral shapes of data sets collected in August 2006, November 2007, November 2008, and April 2009, the $R_{\rm rs}$'s were classified into four types (i.e., A to D) (Fig. 3). The classification criteria were elaborated by comparing the $R_{\rm rs}$ spectra of MERIS bands (Fig. 4).

Type A had high reflectance in NIR, and the spectra showed properties of green vegetation because of the floating algae or aquatic plants; Type B almost had flat curve from bands 5 to 9. This water type usually had higher $C_{\rm tsm}$ and lower $C_{\rm chla}$ compared with other waters (Table II); Type C had two spectral peaks at bands 5 and 9, and the peak at band 5 (555–565 nm) was attributed to low chlorophyll absorption, while band 9 (703.75–713.75 nm) is the combined effect of decreasing absorption by chlorophyll a and increasing absorption by water and scattering by algal cells [7], [39]; the spectra of type D declined from bands 5 to 9 with unobvious reflectance peak. The statistics of $C_{\rm chla}$ and $C_{\rm tsm}$ are shown in Table II.

### C. $C_{\rm chla}$ Retrieving Model Construction

Owing to the presence of floating algae or aquatic plants on type A water surface, the remote sensing signals from water columns under the surface sometimes could not reach the remote sensing sensor. In that case, it was unreasonable to inverse $C_{\rm chla}$ by $R_{\rm rs}$ formed mainly by floating algae or aquatic plants. Meanwhile, in type B water, the signal from suspended matter was much stronger than chlorophyll (e.g., mean $C_{\rm chla}$ was 6.67 mg $\cdot$ m$^{-3}$, whereas mean $C_{\rm tsm}$ was 192.78 mg $\cdot$ L$^{-1}$ in Table II), and the strong absorption of phycocyanin at 625 nm and the reflectance peak near 709 nm were covered up by nonpigment suspended matter scattering.

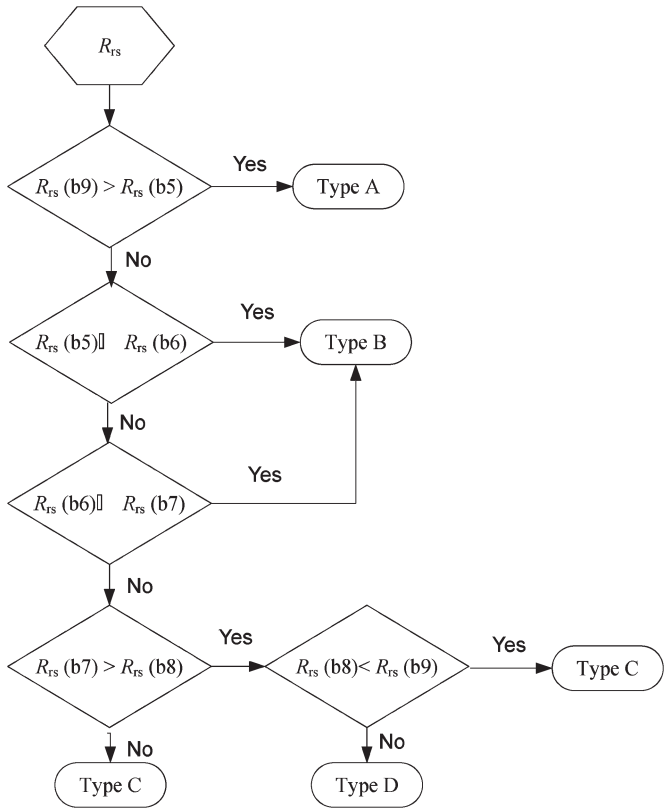


Fig. 4. Classification criteria ($R_{\rm rs}$(b$i$) is $R_{\rm rs}$ of MERIS band $i$, $i = 5, \ldots, 9$; types A to D are water types.)

Consequently, the mixed spectra were not adequate to derive $C_{\rm chla}$. Therefore, our $C_{\rm chla}$ retrieval models were constructed for types C and D waters based on *in situ* measured 2007 and 2008 data sets.

In this paper, the red–NIR bands were used to construct the models [14], [16], and the performances of different band combinations, including $R_{\rm rs}(1) = (R_{\rm rs}^{-1}({\rm b7}) - R_{\rm rs}^{-1}({\rm b9}))R_{\rm rs}({\rm b10})$, $R_{\rm rs}(2) = (R_{\rm rs}^{-1}({\rm b7}) - R_{\rm rs}^{-1}({\rm b9}))(R_{\rm rs}^{-1}({\rm b10}) - R_{\rm rs}^{-1}({\rm b9}))^{-1}$, $R_{\rm rs}(3) = (R_{\rm rs}^{-1}({\rm b8}) - R_{\rm rs}^{-1}({\rm b9}))R_{\rm rs}({\rm b10})$, $R_{\rm rs}(4) = (R_{\rm rs}^{-1}({\rm b8}) - R_{\rm rs}^{-1}({\rm b9}))(R_{\rm rs}^{-1}({\rm b10}) - R_{\rm rs}^{-1}({\rm b9}))^{-1}$, $R_{\rm rs}({\rm b9/b7}) = R_{\rm rs}({\rm b9})/R_{\rm rs}({\rm b7})$, and $R_{\rm rs}({\rm b9/b8}) = R_{\rm rs}({\rm b9})/R_{\rm rs}({\rm b8})$ (b$i$ is band $i$ of MERIS, $i = 7, \ldots, 10$), were compared among each other. Moreover, the regression functions such as linear, power, logarithm, and polynomial were tested. The formulas which performed better than other forms are as follows:

Type C:

$$C_{\rm chla} = 117.9R_{\rm rs}(1) + 15.92 \quad R^2 = 0.738$$
$$MAPE = 25.77\% \quad RMSE = 5.55 \quad N = 39 \tag{7}$$
$$C_{\rm chla} = 46.81R_{\rm rs}(2) + 16.59 \quad R^2 = 0.738$$
$$MAPE = 26.36\% \quad RMSE = 5.54 \quad N = 39 \tag{8}$$
$$C_{\rm chla} = 86.56R_{\rm rs}(3) + 13.30 \quad R^2 = 0.679$$
$$MAPE = 29.05\% \quad RMSE = 6.14 \quad N = 39 \tag{9}$$
$$C_{\rm chla} = 35.52R_{\rm rs}(4) + 14.38 \quad R^2 = 0.717$$
$$MAPE = 28.17\% \quad RMSE = 5.77 \quad N = 39 \tag{10}$$

TABLE II
DESCRIPTIVE STATISTICS OF THE $C_{\mathrm{chla}}$ AND $C_{\mathrm{tsm}}$ [SD: STANDARD DEVIATION; CV: COEFFICIENT OF VARIATION IN PERCENT (i.e., SD/Mean of Parameter)]

| | | Number | Statistics | Minimum | Maximum | Mean | SD | CV (%) |
|---|---|---|---|---|---|---|---|---|
| Type A | All datasets | 14 | $C_{\mathrm{chla}}$(mg m$^{-3}$) | 17.23 | 408.69 | 186.52 | 150.91 | 80.91 |
| | | | $C_{\mathrm{tsm}}$(mg l$^{-1}$) | 21.2 | 143.27 | 74.73 | 42.60 | 57.01 |
| Type B | All datasets | 10 | $C_{\mathrm{chla}}$(mg m$^{-3}$) | 5.36 | 9.28 | 6.67 | 1.34 | 20.09 |
| | | | $C_{\mathrm{tsm}}$(mg l$^{-1}$) | 132.3 | 244.9 | 192.78 | 38.64 | 20.04 |
| Type C | 2007-2008 datasets | 39 | $C_{\mathrm{chla}}$(mg m$^{-3}$) | 4.85 | 65.15 | 22.81 | 13.50 | 59.17 |
| | | | $C_{\mathrm{tsm}}$(mg l$^{-1}$) | 13.33 | 118.67 | 40.06 | 27.88 | 69.59 |
| | 2006 dataset | 17 | $C_{\mathrm{chla}}$(mg m$^{-3}$) | 16.09 | 131.27 | 47.28 | 32.80 | 69.39 |
| | | | $C_{\mathrm{tsm}}$(mg l$^{-1}$) | 7.47 | 84.47 | 42.72 | 21.82 | 51.07 |
| | 2009 dataset | 13 | $C_{\mathrm{chla}}$(mg m$^{-3}$) | 15.90 | 79.80 | 32.77 | 20.99 | 64.07 |
| | | | $C_{\mathrm{tsm}}$(mg l$^{-1}$) | 27.85 | 127.70 | 49.49 | 27.18 | 54.93 |
| Type D | 2007-2008 datasets | 64 | $C_{\mathrm{chla}}$(mg m$^{-3}$) | 0.96 | 47.01 | 8.57 | 6.52 | 76.00 |
| | | | $C_{\mathrm{tsm}}$(mg l$^{-1}$) | 6.27 | 154.67 | 36.49 | 31.22 | 85.57 |
| | 2006 dataset | 23 | $C_{\mathrm{chla}}$(mg m$^{-3}$) | 4.69 | 26.98 | 12.94 | 5.93 | 45.82 |
| | | | $C_{\mathrm{tsm}}$(mg l$^{-1}$) | 6.47 | 58.8 | 25.08 | 12.90 | 51.43 |
| | 2009 dataset | 34 | $C_{\mathrm{chla}}$(mg m$^{-3}$) | 2.98 | 18.67 | 7.64 | 3.94 | 51.64 |
| | | | $C_{\mathrm{tsm}}$(mg l$^{-1}$) | 11.4 | 141.8 | 53.34 | 37.28 | 69.89 |

$$C_{\mathrm{chla}} = 62.83R_{\mathrm{rs}}(\mathrm{b9/b7}) - 47.06 \quad R^2 = 0.683$$
$$MAPE = 26.88\% \quad RMSE = 6.11 \quad N = 39 \qquad (11)$$
$$C_{\mathrm{chla}} = 44.46R_{\mathrm{rs}}(\mathrm{b9/b8}) - 31.44 \quad R^2 = 0.585$$
$$MAPE = 31.08\% \quad RMSE = 6.98 \quad N = 39. \qquad (12)$$

Type D:

$$C_{\mathrm{chla}} = 25.40e^{19.62R_{\mathrm{rs}}(1)} \quad R^2 = 0.619$$
$$MAPE = 38.12\% \quad RMSE = 3.08 \quad N = 64 \qquad (13)$$
$$C_{\mathrm{chla}} = 17.23e^{7.656R_{\mathrm{rs}}(2)} \quad R^2 = 0.325$$
$$MAPE = 54.42\% \quad RMSE = 3.71 \quad N = 64 \qquad (14)$$
$$C_{\mathrm{chla}} = 17.14e^{19.58R_{\mathrm{rs}}(3)} \quad R^2 = 0.658$$
$$MAPE = 35.19\% \quad RMSE = 3.00 \quad N = 64 \qquad (15)$$
$$C_{\mathrm{chla}} = 15.05e^{9.437R_{\mathrm{rs}}(4)} \quad R^2 = 0.477$$
$$MAPE = 45.85\% \quad RMSE = 3.29, N = 64 \qquad (16)$$
$$C_{\mathrm{chla}} = 0.016e^{7.144R_{\mathrm{rs}}(\mathrm{b9/b7})} \quad R^2 = 0.725$$
$$MAPE = 30.56\% \quad RMSE = 2.99 \quad N = 64 \qquad (17)$$
$$C_{\mathrm{chla}} = 009e^{7.435R_{\mathrm{rs}}(\mathrm{b9/b8})} \quad R^2 = 0.742$$
$$MAPE = 29.01\% \quad RMSE = 2.89 \quad N = 64. \qquad (18)$$

### D. Model Validation by In Situ Data

The $R_{\mathrm{rs}}$ measured in 2006 and 2009 was classified according to the classification criteria. Then, $C_{\mathrm{chla}}$ was computed by the aforementioned models for types C and D waters (Table III).

### E. Model Validation by MERIS Data

After atmospheric correction, the MERIS FR imagery data, acquired on November 11, 2007 and November 20, 2008, were classified according to the classification criteria. Then, the $C_{\mathrm{chla}}$ of types C and D was retrieved using functions (7)–(18). The *MAPEs* and *RMSEs* of different models are shown in Table IV.

TABLE III
COMPARISON OF DIFFERENT NIR/RED MODELS FROM 2006 AND 2009 DATA SETS ($R_{\mathrm{rs}}(1) = (R_{\mathrm{rs}}^{-1}(\mathrm{b7}) - R_{\mathrm{rs}}^{-1}(\mathrm{b9}))R_{\mathrm{rs}}(\mathrm{b10})$, $R_{\mathrm{rs}}(2) = (R_{\mathrm{rs}}^{-1}(\mathrm{b7}) - R_{\mathrm{rs}}^{-1}(\mathrm{b9}))(R_{\mathrm{rs}}^{-1}(\mathrm{b10}) - R_{\mathrm{rs}}^{-1}(\mathrm{b9}))^{-1}$, $R_{\mathrm{rs}}(3) = (R_{\mathrm{rs}}^{-1}(\mathrm{b8}) - R_{\mathrm{rs}}^{-1}(\mathrm{b9}))R_{\mathrm{rs}}(\mathrm{b10})$, $R_{\mathrm{rs}}(4) = (R_{\mathrm{rs}}^{-1}(\mathrm{b8}) - R_{\mathrm{rs}}^{-1}(\mathrm{b9}))(R_{\mathrm{rs}}^{-1}(\mathrm{b10}) - R_{\mathrm{rs}}^{-1}(\mathrm{b9}))^{-1}$), $R_{\mathrm{rs}}(\mathrm{b9/b7}) = R_{\mathrm{rs}}(\mathrm{b9})/R_{\mathrm{rs}}(\mathrm{b7})$, AND $R_{\mathrm{rs}}(\mathrm{b9/b8}) = R_{\mathrm{rs}}(\mathrm{b9})/R_{\mathrm{rs}}(\mathrm{b8})$)

| | | 2006 dataset | | 2009 dataset | |
|---|---|---|---|---|---|
| Model | Statistics | Type C | Type D | Type C | Type D |
| | | *N*=17 | *N*=23 | *N*=13 | *N*=34 |
| $R_{\mathrm{rs}}(1)$ | *MAPE* (%) | 35.58 | 38.31 | 27.78 | 34.66 |
| | *RMSE* (mg m$^{-3}$) | 16.42 | 6.93 | 11.69 | 2.71 |
| $R_{\mathrm{rs}}(2)$ | *MAPE* (%) | 76.27 | 38.01 | 26.44 | 31.14 |
| | *RMSE* (mg m$^{-3}$) | 191.86 | 7.09 | 12.93 | 2.72 |
| $R_{\mathrm{rs}}(3)$ | *MAPE* (%) | 33.58 | 38.04 | 28.07 | 26.07 |
| | *RMSE* (mg m$^{-3}$) | 16.01 | 6.53 | 13.45 | 2.17 |
| $R_{\mathrm{rs}}(4)$ | *MAPE* (%) | 77.44 | 37.19 | 27.09 | 24.34 |
| | *RMSE* (mg m$^{-3}$) | 196.70 | 6.63 | 14.34 | 2.29 |
| $R_{\mathrm{rs}}$ | *MAPE* (%) | 39.73 | 43.02 | 26.11 | 41.90 |
| (b9/b7) | *RMSE* (mg m$^{-3}$) | 24.21 | 7.97 | 10.26 | 3.31 |
| $R_{\mathrm{rs}}$ | *MAPE* (%) | 38.34 | 41.03 | 27.98 | 32.58 |
| (b9/b8) | *RMSE* (mg m$^{-3}$) | 25.02 | 7.25 | 12.87 | 2.61 |

For the image data, the performances of the models are not as good as that for *in situ* data, with *MAPEs* larger than 55% and *RMSEs* larger than 8 mg $\cdot$ m$^{-3}$. On the other hand, when evaluating the estimation accuracies by different $C_{\mathrm{chla}}$ ranges, the accuracies were acceptable when $C_{\mathrm{chla}} > 5$ mg $\cdot$ m$^{-3}$ (Table V).

To further assess the accuracies of the algorithms, the 13 stations collected in the same day with image acquisition were selected for match-up comparison. Fig. 5 shows the retrieved and measured values at these stations. The $C_{\mathrm{chla}}$

TABLE IV
COMPARISON OF DIFFERENT NIR/RED MODELS FROM 2007 AND 2008 MERIS DATA ($R_{\rm rs}(1) = (R_{\rm rs}^{-1}(\text{b7}) - R_{\rm rs}^{-1}(\text{b9}))R_{\rm rs}(\text{b10})$, $R_{\rm rs}(2) = (R_{\rm rs}^{-1}(\text{b7}) - R_{\rm rs}^{-1}(\text{b9}))(R_{\rm rs}^{-1}(\text{b10}) - R_{\rm rs}^{-1}(\text{b9}))^{-1}$, $R_{\rm rs}(3) = (R_{\rm rs}^{-1}(\text{b8}) - R_{\rm rs}^{-1}(\text{b9}))R_{\rm rs}(\text{b10})$, $R_{\rm rs}(4) = (R_{\rm rs}^{-1}(\text{b8}) - R_{\rm rs}^{-1}(\text{b9}))(R_{\rm rs}^{-1}(\text{b10}) - R_{\rm rs}^{-1}(\text{b9}))^{-1})$, $R_{\rm rs}(\text{b9/b7}) = R_{\rm rs}(\text{b9})/R_{\rm rs}(\text{b7})$, AND $R_{\rm rs}(\text{b9/b8}) = R_{\rm rs}(\text{b9})/R_{\rm rs}(\text{b8})$)

| Model | Statistics | Type C | Type D | Model | Statistics | Type C | Type D |
|---|---|---|---|---|---|---|---|
| $R_{\rm rs}(1)$ | *MAPE* (%) | 66.73 | 61.61 | $R_{\rm rs}(4)$ | *MAPE* (%) | 71.85 | 64.75 |
| | *RMSE* (mg m$^{-3}$) | 8.75 | 10.65 | | *RMSE* (mg m$^{-3}$) | 8.99 | 10.99 |
| $R_{\rm rs}(2)$ | *MAPE* (%) | 69.93 | 61.68 | $R_{\rm rs}$(b9/b7) | *MAPE* (%) | 65.30 | 58.04 |
| | *RMSE* (mg m$^{-3}$) | 8.78 | 11.04 | | *RMSE* (mg m$^{-3}$) | 8.75 | 9.89 |
| $R_{\rm rs}(3)$ | *MAPE* (%) | 68.49 | 65.78 | $R_{\rm rs}$(b9/b8) | *MAPE* (%) | 67.97 | 61.91 |
| | *RMSE* (mg m$^{-3}$) | 8.88 | 10.61 | | *RMSE* (mg m$^{-3}$) | 8.81 | 10.00 |

TABLE V
COMPARISON OF MODEL $R_{\rm rs}$ (b9/b7) FROM DIFFERENT $C_{\rm chla}$ RANGES

| Range | *MAPE* (%) | *RMSE* (mg m$^{-3}$) |
|---|---|---|
| 0 mg m$^{-3}$< $C_{\rm chla}$ <=5 mg m$^{-3}$ | 106.23 | 5.02 |
| 5 mg m$^{-3}$< $C_{\rm chla}$ <=10 mg m$^{-3}$ | 56.79 | 4.45 |
| 10 mg m$^{-3}$< $C_{\rm chla}$ <=20 mg m$^{-3}$ | 38.04 | 5.59 |
| 20 mg m$^{-3}$< $C_{\rm chla}$ <=30 mg m$^{-3}$ | 33.80 | 8.72 |
| 30 mg m$^{-3}$< $C_{\rm chla}$ | 58.74 | 32.55 |

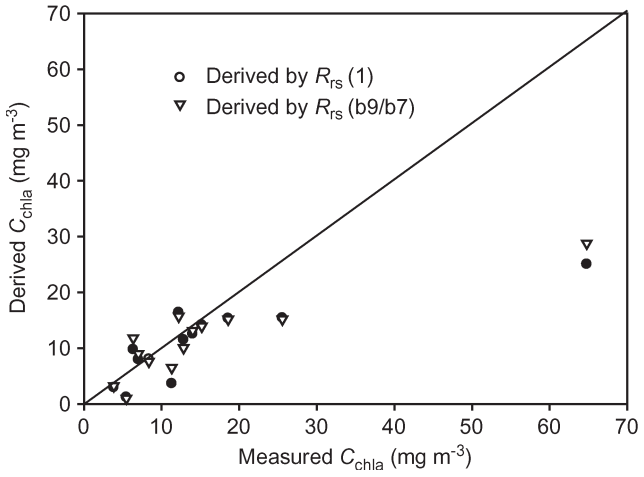


Fig. 5. Measured and derived $C_{\rm chla}$ of the stations in which the *in situ* and image data were collected at the same day.

ranged from 3.84 to 64.78 mg $\cdot$ m$^{-3}$. When we eliminated one station which had the highest percent difference of 279.32% via $R_{\rm rs}(\text{b9}/\text{b7})$, the *MAPE* was 29.96%, and the *RMSE* was 4.28 mg $\cdot$ m$^{-3}$. Although they were fetched at the same day, the data were still not exactly matched because it took several hours to collect *in situ* data, whereas the satellite captured its entire swath just within a few seconds. Therefore, taking the time difference and spatial resolution into consideration, the accuracy is acceptable for retrieving $C_{\rm chla}$ in inland eutrophic waters.

Fig. 6 shows the retrieved values of $C_{\rm chla}$ in 2007 and 2008 through $R_{\rm rs}$ (b9/b7). It can be concluded that the $C_{\rm chla}$ mainly ranged from 0 to 20 mg $\cdot$ m$^{-3}$, e.g., 0 mg $\cdot$ m$^{-3}$ $< C_{\rm chla} \leq$ 20 mg $\cdot$ m$^{-3}$ accounted for 83.70% area in 2007 image data, while the area was 86.63% in 2008 image.

## IV. DISCUSSION AND CONCLUSION

The universal algorithms for retrieving $C_{\rm chla}$ from ocean color images have been commonly used [2], [5]. However, for coastal and inland waters, retrieving $C_{\rm chla}$ has always been a problem because of the complexity of water optical properties. In the present study, we tried to classify Taihu Lake into different water types according to their different water optical properties and then established $C_{\rm chla}$ retrieving algorithms based on the water types.

### A. Possibility of Water Classification

The classical scheme of Morel and Prieur [40] classifies natural waters into two types, i.e., Case-1 waters which were optically dominated by phytoplankton and their degradation products and Case-2 waters which were dominated by other optically active constituents (OACs) as well as phytoplankton. This classification scheme is actually a simplification of all natural water types, because it treats all non-Case-1 waters as Case-2, though realizing the presence of optical differences among the Case-2 waters. However, inland waters, or so-called Case-2 waters, might present very different optical properties, when dominated by one or more of the following OACs: phytoplankton, colored dissolved organic matter, and suspended matter [21]–[23], [42]. Because of the various proportions of the OACs in contributing to the reflectance, the preclassification is often necessary for parameter retrievals by remotely sensed data [42].

The classification scheme proposed in this paper mainly depends on the relative magnitude of $R_{\rm rs}$ by comparing the

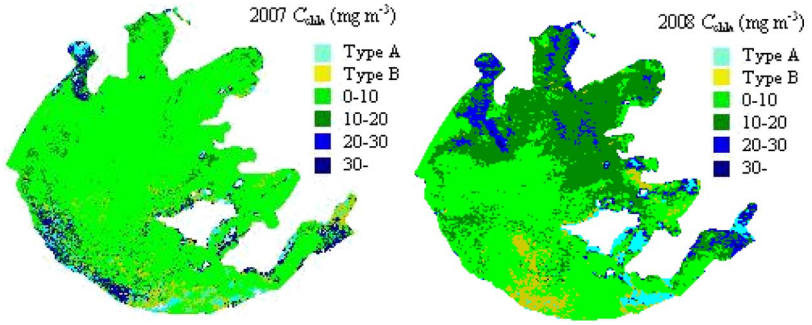


Fig. 6. $C_{\mathrm{chla}}$ retrieved by $R_{\mathrm{rs}}$ (b9/b7) models from MERIS FR images acquired on November 11, 2007 and November 20, 2008. Type A includes floating algae and plants; type B has very high $C_{\mathrm{tsm}}$ and low $C_{\mathrm{chla}}$ (i.e., $C_{\mathrm{tsm}} > 100$ mg $\cdot$ L$^{-1}$, while $C_{\mathrm{chla}} < 10$ mg $\cdot$ m$^{-3}$).

TABLE VI
PERCENTAGE OF WATER TYPES CLASSIFIED BY IMAGE DATA (IN PERCENT) (2007: IMAGE DATA ON NOVEMBER 11, 2007; 2008: IMAGE DATA ON NOVEMBER 20, 2008)

| | Type A | Type B | Type C | Type D |
|---|---|---|---|---|
| 2007 | 3.21 | 5.04 | 14.09 | 77.66 |
| 2008 | 3.58 | 4.93 | 33.10 | 58.39 |

values from bands 5 to 9, which ensures the possibility of identifying every $R_{\mathrm{rs}}$ spectrum into one of the four classes. Table VI shows the percentage of water types in 2007 and 2008. It could be observed that type D is the dominant water type in Taihu Lake, and the next one is type C, although the percentages of different water types changed within a year. This illustrates significant spatial–temporal variations in water types. Moreover, this necessitates the use of type-specific models for estimating $C_{\mathrm{chla}}$.

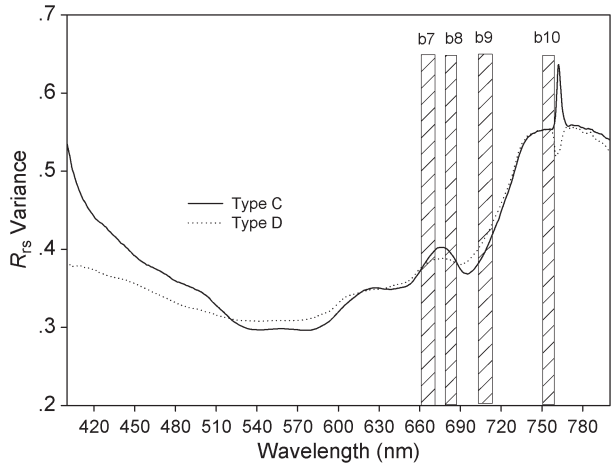


Fig. 7. $R_{\mathrm{rs}}$ variance of types C and D waters.

### B. Comparison of the Different Models

According to previous researches [6]–[8], [10], [12]–[14], [41], the NIR/red ratio model, three-band model, and four-band model were constructed for retrieving $C_{\mathrm{chla}}$. The models were composed of six kinds of band combinations, i.e., $R_{\mathrm{rs}}(1) = (R_{\mathrm{rs}}^{-1}(\mathrm{b7}) - R_{\mathrm{rs}}^{-1}(\mathrm{b9}))R_{\mathrm{rs}}(\mathrm{b10})$, $R_{\mathrm{rs}}(2) = (R_{\mathrm{rs}}^{-1}(\mathrm{b7}) - R_{\mathrm{rs}}^{-1}(\mathrm{b9}))(R_{\mathrm{rs}}^{-1}(\mathrm{b10}) - R_{\mathrm{rs}}^{-1}(\mathrm{b9}))^{-1}$, $R_{\mathrm{rs}}(3) = (R_{\mathrm{rs}}^{-1}(\mathrm{b8}) - R_{\mathrm{rs}}^{-1}(\mathrm{b9}))R_{\mathrm{rs}}(\mathrm{b10})$, $R_{\mathrm{rs}}(4) = (R_{\mathrm{rs}}^{-1}(\mathrm{b8}) - R_{\mathrm{rs}}^{-1}(\mathrm{b9})) \times (R_{\mathrm{rs}}^{-1}(\mathrm{b10}) - R_{\mathrm{rs}}^{-1}(\mathrm{b9}))^{-1}$, $R_{\mathrm{rs}}(\mathrm{b9/b7}) = R_{\mathrm{rs}}(\mathrm{b9})/R_{\mathrm{rs}}(\mathrm{b7})$, and $R_{\mathrm{rs}}(\mathrm{b9/b8}) = R_{\mathrm{rs}}(\mathrm{b9})/R_{\mathrm{rs}}(\mathrm{b8})$.

For the 2007–2008 data sets, which were used for model construction, there were no significant differences among the six models in type C water. However, $R_{\mathrm{rs}}(1)$, $R_{\mathrm{rs}}(2)$, and $R_{\mathrm{rs}}(\mathrm{b9/b7})$ performed better with relatively low *MAPE* and *RMSE*. The $R_{\mathrm{rs}}(\mathrm{b9/b7})$ and $R_{\mathrm{rs}}(\mathrm{b9/b8})$ got lowest *MAPE* and *RMSE* in type D water. In addition, the three-band models were better than four-band models in this water type. For the *in situ* validation data sets, i.e., 2006 and 2009 data sets, the models had very different performances. Three-band $R_{\mathrm{rs}}(3)$ and four-band $R_{\mathrm{rs}}(4)$ performed well in type D water of 2006 data set. However, for type C water, four-band $R_{\mathrm{rs}}(2)$ and $R_{\mathrm{rs}}(4)$ had a poor performance, because that the *MAPEs*, and *RMSEs* are twice larger than other models when using the 2006 data set. Moreover, in this data set, three-band $R_{\mathrm{rs}}(1)$ and $R_{\mathrm{rs}}(3)$ were better than two-band ratio models. There were no significant differences in 2009 data set. For image data, two-band ratio and three-band $R_{\mathrm{rs}}(1)$ could obtain relatively low *MAPE* and *RMSE* values. Bands 7 and 8 did not have significant differences in the model construction, partly due to the stable $R_{\mathrm{rs}}$ variance at these two bands (Fig. 7). As we know, band 8 is affected by chlorophyll a fluorescence, and there is a general understanding that the quantum yield of fluorescence can vary with $C_{\mathrm{chla}}$. Nevertheless, this variation of quantum yield might depend on phytoplankton species, and when that happens, the fluorescence band cannot be reliably used for estimating $C_{\mathrm{chla}}$. In our data set, there is no apparent variation of the fluorescence quantum yield, which has resulted in reasonably good results when using models involving band 8. However, the same models may not yield results with comparable accuracies when applied to waters where the fluorescence quantum yield is significantly variable.

The regression trends were different between types C and D. For type C water, $\boldsymbol{C_{\mathbf{chla}}}$ is linearly related with the combined $R_{\mathrm{rs}}$, while power functions performed well for describing the relationship of $C_{\mathrm{chla}}$ and combined $R_{\mathrm{rs}}$ for type D water.

To sum up, both three-band model and two-band ratio model could be utilized for *in situ* data and image data in Taihu Lake. Moreover, bands 7 and 9 combination was better than that of bands 8 and 9. Therefore, we suggest a two-band ratio model for retrieving $C_{\mathrm{chla}}$ from image data with two reasons: 1) to avoid error accumulation from atmospheric correction by more bands and 2) to minimize atmospheric correction error through band ratio [6].

## ACKNOWLEDGMENT

The authors would like to thank Dr. Z. Lee from Mississippi State University and Dr. C. Hu from the University of South Florida for their support and the European Space Agency Envisat for providing the Medium Resolution Imaging Spectrometer data. The authors would also like to thank L. Wu, X. Wang, K. Shi, R. Xia, Y. Yang, X Jin, Y. F. Wang, H. Zhang, Y. F. Xu, X. Xu, and Z. H. Liu for their participation in the field experiment; the two anonymous reviewers for their constructive comments and suggestions; and X. Zhou and D. Sun for revising the English usage.

## REFERENCES

[1] H. R. Gordon and A. Morel, *Remote Assessment of Ocean Color for Interpretation of Satellite Visible Imagery, A Review*. New York: Springer-Verlag, 1983.

[2] J. E. O'Reilly, S. Maritorena, B. G. Mitchell, D. A. Siegel, K. L. Carder, S. A. Garver, M. Kahru, and C. McClain, "Ocean color chlorophyll algorithms for SeaWiFS," *J. Geophys. Res.*, vol. 103, no. C11, pp. 24 937–24 953, Oct. 1998.

[3] J. L. Mueller and R. W. Austin, "Ocean optics protocols for SeaWiFS validation, revision 1," in *NASATech. Memo. 104 566*, S. B. Hooker, E. R. Firestone, and J. G. Acker, Eds. Greenbelt, MD: NASA Goddard Space Flight Center, 1995, 66 pp..

[4] K. L. Carder, F. R. Chen, J. P. Cannizzaro, J. W. Campbell, and B. G. Mitchell, "Performance of the MODIS semi-analytical ocean color algorithm for chlorophyll-a," *Adv. Space Res.*, vol. 33, no. 7, pp. 1152–1159, Jan. 2004.

[5] M. Darecki and D. Stramski, "An evaluation of MODIS and SeaWiFS bio-optical algorithms in the Baltic Sea," *Remote Sens. Environ.*, vol. 89, no. 3, pp. 326–350, Feb. 2004.

[6] G. Dall'Olmoa, A. A. Gitelsona, D. C. Rundquista, B. Leavitta, T. Barrow, and J. C. Holz, "Assessing the potential of SeaWiFS and MODIS for estimating chlorophyll concentration in turbid productive waters using red and near-infrared bands," *Remote Sens. Environ.*, vol. 96, no. 2, pp. 176–187, May 2005.

[7] A. A. Gitelson, "The peak near 700 nm on reflectance spectra of algae and water: Relationships of its magnitude and position with chlorophyll concentration," *Int. J. Remote Sens.*, vol. 13, no. 17, pp. 3367–3373, 1992.

[8] H. J. Gons, "Optical teledetection of chlorophyll a in turbid inland waters," *Environ. Sci. Technol.*, vol. 33, no. 7, pp. 1127–1132, Apr. 1999.

[9] J. F. R. Gower, R. Doerffer, and G. A. Borstad, "Interpretation of the 685 nm peak in water-leaving radiance spectra in terms of fluorescence, absorption and scattering, and its observation by MERIS," *Int. J. Remote Sens.*, vol. 20, pp. 1771–1786, 1999.

[10] H. J. Gons, M. Rijkeboer, and K. G. Ruddick, "Effect of a waveband shift on chlorophyll retrieval from MERIS imagery of inland and coastal waters," *J. Plankton Res.*, vol. 27, no. 1, pp. 125–127, Jan. 2005.

[11] G. Dall'Olmo and A. A. Gitelson, "Effect of bio-optical parameter variability on the remote estimation of chlorophyll-a concentration in turbid productive waters: Experimental results," *Appl. Opt.*, vol. 44, no. 3, pp. 412–422, Jan. 2005.

[12] W. J. Moses, A. A. Gitelson, S. Berdnikov, and V. Povazhnyy, "Satellite estimation of chlorophyll-a concentration using the red and NIR bands of MERIS—The Azov Sea case study," *IEEE Geosci. Remote Sens. Lett.*, vol. 6, no. 4, pp. 845–849, Oct. 2009.

[13] A. A. Gitelson, J. F. Schalles, and C. M. Hladik, "Remote chlorophyll-a retrieval in turbid, productive estuaries: Cheapeake Bay case study," *Remote Sens. Environ.*, vol. 109, no. 4, pp. 464–472, Aug. 2007.

[14] A. A. Gitelson, G. Dall'Olmo, W. Moses, D. C. Rundquist, T. Barrow, T. R. Fisher, D. Gurlin, and J. Holz, "A simple semi-analytical model for remote estimation of chlorophyll-a in turbid waters: Validation," *Remote Sens. Environ.*, vol. 112, no. 9, pp. 3582–3593, Sep. 2008.

[15] P. V. Zimba and A. A. Gitelson, "Remote estimation of chlorophyll concentration in hyper-eutrophic aquatic systems: Model tuning and accuracy optimization," *Aquaculture*, vol. 256, no. 1–4, pp. 272–286, Jun. 2006.

[16] C. F. Le, Y. M. Li, Y. Zha, D. Y. Sun, C. C. Huang, and H. Lu, "A four-band semi-analytical model for estimating chlorophyll a in highly turbid lakes: The case of Taihu Lake, China," *Remote Sens. Environ.*, vol. 113, no. 6, pp. 1175–1182, Jun. 2009.

[17] D. Y. Sun, Y. M. Li, and Q. Wang, "A unified model for remotely estimating chlorophyll a in Lake Taihu, China, based on SVM and in situ hyperspectral data," *IEEE Trans. Geosci. Remote Sens.*, vol. 47, no. 8, pp. 2957–2965, Aug. 2009.

[18] G. H. Zhou, Q. H. Liu, R. H. Ma, and G. L. Tang, "Inversion of chlorophyll-a concentration in turbid water of Lake Taihu based on optimized multi-spectral combination," *J. Lake Sci.*, vol. 20, no. 2, pp. 153–159, Mar. 2008.

[19] *MERIS Product Handbook*, ESA, Paris, France, 2007, Issue 2.1.

[20] M. Rast, "The ESA medium resolution imaging spectrometer MERIS—A review of the instrument and its mission," *Int. J. Remote Sens.*, vol. 20, no. 9, pp. 1681–1720, 1999.

[21] F. A. Vertucci and G. E. Likens, "Spectral reflectance and water quality of Adirondack mountain region lakes," *Limnol. Oceanogr.*, vol. 34, no. 8, pp. 1656–1672, Dec. 1989.

[22] S. Kaczmarek and B. Wozniak, "The application of the optical classification of the waters in the Baltic Sea (case 2 waters)," *Oceanologia*, vol. 37, no. 2, pp. 285–297, 1995.

[23] G. C. Chang, A. H. Barnard, S. McLean, P. J. Egli, C. Moore, J. R. V. Zaneveld, T. D. Dickey, and A. Hanson, "*In situ* optical variability and relationships in the Santa Barbara Channel: Implications for remote sensing," *Appl. Opt.*, vol. 45, no. 15, pp. 3593–3604, May 2006.

[24] D. Y. Sun, Y. M. Li, C. C. Le, S. Q. Gong, L. Wu, and C. C. Huang, "Scattering characteristics of Taihu Lake and its relationship models with suspended particle concentration," *Environ. Sci.*, vol. 28, no. 12, pp. 2688–2694, Dec. 2007.

[25] A. Morel, B. Gentili, M. Chami, and J. Ras, "Bio-optical properties of high chlorophyll Case 1 waters and of yellow-substance-dominated Case 2 waters," *Deep-Sea Res. Part 1—Oceanogr. Res. Papers*, vol. 53, no. 9, pp. 1439–1459, Sep. 2006.

[26] B. Q. Qin, W. P. Hu, and W. M. Chen, *The Process and Mechanism of Water Environment Evolvement in Taihu Lake*. Beijing, China: Sci. Press, 2004, pp. 1–2.

[27] C. M. Hu, Z. P. Lee, R. H. Ma, K. Yu, D. Q. Li, and S. L. Shang, "MODIS observations of cyanobacteria blooms in Taihu Lake, China," *J. Geophys. Res.*, vol. 115, p. C04 002, Apr. 2010. DOI:10.1029/2009JC005511.

[28] J. L. Mueller, A. Morel, R. Frouin, C. Davis, R. Arnone, K. Carder, Z. P. Lee, R. G. Steward, S. Hooker, C. D. Mobley, S. McLean, B. Holben, M. Miller, C. Pietras, K. D. Knobelspiesse, G. S. Fargion, J. Porter, and K. Voss, *Ocean Optics Protocols for Satellite Ocean Color Sensor Validation*. Greenbelt, MD: GSFC, 2003, Revision 4.

[29] C. D. Mobley, "Estimation of the remote sensing reflectance from above-surface measurements," *Appl. Opt.*, vol. 38, no. 36, pp. 7442–7455, Dec. 1999.

[30] X. Huang, *Eco-Investigation, Observation and Analysis of Lakes*. Beijing, China: Standard Press China, 1999, pp. 77–99.

[31] N. A. Welschmeyer, "Fluorometric analysis of chlorophyll a in the presence of chlorophyll B and pheopigments," *Limnol. Oceanogr.*, vol. 39, no. 8, pp. 1985–1992, 1994.

[32] W. J. Moses, A. A. Gitelson, S. Berdnikov, and V. Povazhnyy, "Estimation of chlorophyll-a concentration in case II waters using MODIS and MERIS data—Successes and challenges," *Environ. Res. Lett.*, vol. 4, no. 4, pp. 1–8, Oct./Dec. 2009. DOI: 10.1088/1748-9326/4/4/045005.

[33] H. R. Gordon and M. H. Wang, "Influence of oceanic whitecaps on atmospheric correction of ocean-color sensors," *Appl. Opt.*, vol. 33, no. 33, pp. 7754–7763, Nov. 1994.

[34] K. G. Ruddick, F. Ovidio, and M. Rijkeboer, "Atmospheric correction of SeaWiFS imagery for turbid coastal and inland waters," *Appli. Opt.*, vol. 39, no. 6, pp. 897–912, Feb. 2000.

[35] T. H. Schroeder, I. Behnert, M. Schaale, J. Fischer, and R. Doerffer, "Atmospheric correction algorithm for MERIS above case-2 waters," *Int. J. Remote Sens.*, vol. 28, no. 7, pp. 1469–1486, Mar. 2007.

[36] R. Doerffer and H. Schiller, "MERIS regional coastal and lake case 2 water project atmospheric correction ATBD," GKSS Research Center, Geesthacht, Germany, Tech. Rep., May 2008.

[37] F. C. Hu, "Remote sensing atmospheric properties of Taihu Lake area by MODIS and sun photometer," Ph.D. dissertation, Inst. Remote Sens. Appl., Chinese Acad. Sci., Beijing, China, 2007.

[38] L. Guanter, A. Ruiz-Verdu, D. Odermatt, C. Giardino, S. Simis, V. Estelles, T. Heege, J. A. Dominguez-Gomez, and J. Moreno, "Atmospheric correction of ENVISAT/MERIS data over inland waters: Validation for European lakes," *Remote Sens. Environ.*, vol. 114, no. 3, pp. 467–480, Mar. 2010.

[39] A. G. Dekker, T. J. Malthus, M. M. Wijnen, and E. Seyhan, "The effect of spectral bandwidth and positioning on the spectral signature analysis of inland waters," *Remote Sens. Environ.*, vol. 41, no. 2/3, pp. 211–225, Feb. 1992.

[40] A. Morel and L. Prieur, "Analysis of variations in ocean color," *Limnol. Oceanogr*, vol. 22, no. 4, pp. 709–722, Jul. 1977.
[41] Y. Z. Yacobi, A. Gitelson, and M. Mayo, "Remote sensing of chlorophyll in Lake Kinneret using highspectral-resolution radiometer and Landsat TM: Spectral features of reflectance and algorithm development," *J. Plankton Res.*, vol. 17, no. 11, pp. 2155–2173, Nov. 1995.
[42] H. Arst and A. Reinart, "Application of optical classifications to North European lakes," *Aquat. Ecol.*, vol. 43, no. 4, pp. 789–801, Dec. 2009. DOI:10.1007/s1045-008-9225-4.

**Yunmei Li** received the B.S. degree in mathematics from the Yunnan University, Kunming, China, in 1987 and the Ph.D. degree in remote sensing technology and application from Zhejiang University, Hangzhou, China, in 2001.

She is currently with Nanjing Normal University, Nanjing, China, where from 2001 to 2003, she was a Postdoctoral Researcher, from 2003 to 2007 was an Associate Professor, and since 2007, has been a Full Professor of remote-sensing technology and applications and currently teaches hyperspectral remote sensing, geographical-information systems, and water-color remote sensing. She is also currently the Head of the Water Color Remote Sensing Laboratory, Department of Geographical Science, Nanjing Normal University. Her current research interests are in the area of water color remote sensing (water component concentration retrieval, inherent optical properties of water bodies, and bio-optical modeling for optically complex waters), particularly for inland turbid lakes. She conducts and supervises research on these topics within the frameworks of several national projects and has been appointed as Evaluator of project proposals. She authored or coauthored more than 60 scientific publications, including journals, book chapters, and conference proceedings.

**Qiao Wang** received the B.S. degree in mathematics from Nankai University, Tianjin, China, in 1982 and the M.S. degree in map science and the Ph.D. degree in geographical information system from Wuhan University, Wuhan, China, in 1992 and 1996, respectively.

From 1992 to 1996, he was an Associate Professor with Wuhan University. From 1996 to 1998, he was a Postdoctoral Researcher with the Institute of Remote Sensing Applications, Chinese Academy of Sciences, Beijing, China. Since 1998, he has been a Researcher with the National Environment Protection Headquarters, Beijing. Since 2010, he has been a Director with the Satellite Environment Application Center, Ministry of Environmental Protection. He has conducted more than 20 projects about research on environment remote sensing, geographical information system, etc., within the national project frameworks and has also been appointed as Evaluator of project proposals. He authored or coauthored more than 80 scientific publications, including journals, books, and conference proceedings.

**Chuanqing Wu** received the B.S. degree in geography from Peking University, Beijing, China, in 1999, the M.S. degree in remote sensing and geographical information system from the Institute of Remote Sensing Applications, Chinese Academy of Sciences, Beijing, in 2002, and the Doctor degree in environmental science from Beijing Normal University, Beijing, in 2008.

Since 2002, he has been a Researcher with the Ministry of Environmental Protection, Beijing. He is currently the Director of Water Remote Sensing Department, Satellite Environment Application Center, Ministry of Environmental Protection. His current research interests are water-color remote sensing and environmental application (water component concentration retrieval, water environmental pollutions, and disease monitoring). He has conducted more than five projects, researching on environment remote sensing. He has authored or coauthored more than 20 scientific publications, including journals, book chapters, and conference proceedings.

**Shaohua Zhao** received the B.S. degree in agronomy from Henan Agricultural University, Zhengzhou, China, in 2002, the M.S. degree in ecology from the Institute of Applied Ecology, Chinese Academy of Sciences, Beijing, China, in 2005, and the Ph.D. degree from Beijing Normal University, Beijing, in 2008.

He was a Postdoctoral Researcher with Peking University, Beijing, from 2008 to 2010. He is currently with the Satellite Environment Application Center, Ministry of Environmental Protection, Beijing. His research interests include ecology and hydrology remote sensing.

**Xing Xu** received the B.S. degree in geographical information system from the Nanjing University of Technology, Nanjing, China, in 2009. Since 2009, she has been working toward the M.S. degree at Nanjing Normal University, Nanjing, where she majored in the field of environment remote sensing.

Her research interests are water-color remote sensing and optical properties in optically complex water bodies.

**Yanfei Wang** received the B.S. degree in geographical information system from Shandong University, Jinan, China, in 2008. Since 2008, he has been working toward the M.S. degree at Nanjing Normal University, Nanjing, China, where he majored in the field of environment remote sensing.

His research interest is atmospheric correction for inland water.

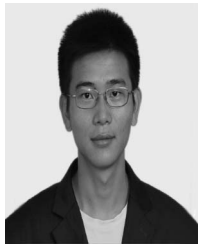

**Changchun Huang** received the B.S. degree in land management from Nanjing Normal University, Nanjing, China, in 2006, where he has been working toward the M.S. and Ph.D. degrees since 2006 and majored in the field of remote sensing technology and applications.

His research interests are water-color remote sensing and water dynamics.